Supplementary Information for the Paper Entitled:

Assessing Structure and Dynamics of Iron Complexes Supported by Tris(amidate)amine Ligands

Lucy S. X. Huffman[1], Anjana Seshadri[2], Christopher D. Hastings[1], William W. Brennessel[1], Ignacio Franco[1,3], and Brandon R. Barnett[1]*

[1]Department of Chemistry, University of Rochester, Rochester, NY 14627
[2]Department of Chemical Engineering, University of Rochester, Rochester, NY 14627
[3]Department of Physics, University of Rochester, Rochester, NY 14627

Email: brandon.barnett@rochester.edu

Contents

S1. General Considerations

All manipulations were carried out under an atmosphere of purified dinitrogen using standard Schlenk and glovebox techniques. Unless otherwise stated, reagent-grade starting materials were purchased from commercial sources and either used as received or purified by standard procedures.[1] The proligand H_3L^{OCH2O} was synthesized as reported previously.[2] The iron(II) complex **[K(Crypt)][FeL^{OCH2O}]** (Crypt = [2.2.2]cryptand) was prepared according to a prior report.[3] Tetrabutylammonium fluoride (TBAF) was synthesized using a literature procedure.[4] Unless otherwise stated, organic solvents were deoxygenated and dried using a Pure Process Technologies solvent purification system. *N,N*-dimethylacetamide (DMA) and dimethyl sulfoxide-*d*$_6$ (DMSO-*d*$_6$) were stored over activated 3 Å molecular sieves, transferred via cannula into a separate flask, sparged with N_2 for 1 h, and stored over fresh 3 Å molecular sieves in the glovebox prior to use. MeCN-*d*$_3$ was refluxed over CaH_2 for several hours before being distilled into a Strauss flask and stored in the glovebox over activated aluminia. Molecular sieves (3 Å), alumina, and Celite were separately pre-activated in a 180 ºC oven overnight, then transferred into a round bottom flask and heated under vacuum ($P < 100$ mTorr) at a temperature in excess of 200 ºC for at least 12 h, and then stored in the glovebox. Tetra(*n*-butylammonium) hexafluorophosphate (electrolyte for electrochemical measurements) was recrystallized three times from ethanol, and then dried under vacuum with P_2O_5 at 120 ºC until the pressure reached 50 mTorr.

Solution ^1H and ^{19}F nuclear magnetic resonance (NMR) spectra were recorded on a Bruker DPX-400 or DPX-500 locked on the signal of deuterated solvents. ^1H chemical shifts are reported in ppm relative to $SiMe_4$ ($\delta = 0.0$ ppm) with reference to residual solvent resonances. ^{19}F chemical shifts are reported in ppm relative to a $PhCF_3$ solution ($\delta = –63.2$ ppm) and were referenced externally. Electronic absorption measurements were recorded using either an Agilent Cary 3500 UV−Vis Engine spectrometer, an Agilent Cary 6000i UV-Vis-NIR spectrometer, or a PerkinEkmer Lambda 35 UV−Vis spectrometer. Samples were prepared in the glovebox and sealed in a quartz cuvette (1 cm pathlength). X-band electron paramagnetic resonance (EPR) measurements were carried out on a Bruker EMXplus spectrometer (microwave frequency of 9.382 GHz). Samples were prepared as solutions or powder in the glovebox, flash-cooled in liquid nitrogen, and loaded into the spectrometer. Fitting of EPR spectral parameters was performed using the EasySpin program.[5] Electrochemical measurements were performed using a CH Instruments 620 D potentiostat with a three-electrode setup, including a $Ag/AgNO_3$ (1 M) reference electrode (CHI111), a Pt wire counter electrode (CHI115, surface area in solution of 0.14 cm^2), and a glassy carbon working electrode (CHI104, 3 mm diameter). Solutions were prepared using dry and degassed DMF or CH_2Cl_2 at a concentration of 1 mM or 10 mM metal complex. The $[NBu_4]PF_6$ electrolyte concentration was 0.1 M. Voltammograms were referenced to the $Cp_2Fe^{+/0}$ couple using ferrocene as an internal standard. Solution phase effective magnetic moments were determined using the Evans method. A dried solid analyte sample was dissolved in 0.800 mL of 9:1 v/v solvent/$PhCF_3$. This solution was added to a borosilicate NMR tube, along with a flame-sealed glass capillary containing a 4:1 v/v solvent/$PhCF_3$ internal standard. Elemental analyses were performed on a PerkinElmer 2400 Series II Analyzer at the CENTC Elemental Analysis Facility, University of Rochester.

S2. Syntheses and Characterization.

Synthesis of ferrocenium triflate (FcOTf). In the glovebox, a 100 mL flat-bottom flask was charged with ferrocene (1.56 g, 8.41 mmol, 1.00 eq.) and silver trifluoromethanesulfonate (2.18 g, 8.50 mmol, 1.01 eq.). THF (25 mL) was added, and the solution was stirred for 2 d. The blue solution with suspended Ag(0) was dried *in vacuo* before being dissolved in 20 mL CH_2Cl_2 and filtered through Celite. The filtrate was layered with 50 mL pentane and stored in a glovebox freezer at –35 ºC for 2 d yielded blue needles, which were harvested and washed with pentane. Yield: 2.70 g, 8.39 mmol, 96%.

Synthesis of [K(18-crown-6)][FeL$^{\mathbf{OMe}}$]. In the glovebox, a scintillation vial was charged with **H$_3$L$^{\mathbf{OMe}}$** (1.0 g, 1.57 mmol) and KH (0.221 g, 5.48 mmol, 3.5 eq.). DMA (7 mL) was added, and the effervescent solution was stirred for 1 h during which time bubbling ceased. This solution was filtered through Celite to remove residual KH, and then added to solid $Fe(OAc)_2$ (0.300 g, 1.72 mmol, 1.1 eq.) and stirred for 3 h. After filtering through Celite, 18-crown-6 (0.455 g, 1.72 mmol, 1.1 eq.) was added and Et_2O was layered to crystallize the desired complex. After decanting the mother liquor, the crystals were washed with a 5:1 Et_2O:DMA solution. The crystals were then redissolved in a minimal volume of DMA and layered with Et_2O to again form crystals. After decanting, the crystals were again washed with a 5:1 Et_2O:DMA solution. This process was repeated once more, followed by three washes of Et_2O to remove residual DMA. The pale green crystals were then dried under vacuum to yield **[K(18-crown-6)][FeL$^{\mathbf{OMe}}$]**. Yield: 0.695 g, 0.70 mmol, 45%. μ_{eff} = 5.8 μ_B (Evans method, ^{19}F NMR, CH_2Cl_2/$PhCF_3$, 23 ºC). Calculated combustion analysis for $C_{45}H_{63}N_4O_{15}FeK$: C, 54.15%; H, 6.36%; N, 5.61%. Found: C, 53.71%; H, 6.12%; N, 5.42%.

Synthesis of FeL$^{\mathbf{OCH2O}}$. In the glovebox, a scintillation vial was charged with FcOTf (20 mg, 61 μmol, 1.0 eq) and 1.5 mL of CH_2Cl_2. The solution was added to a scintillation vial containing solid [K(Crypt)][FeL^{OCH2O}] (64 mg, 60 μmol) and a stir bar and stirred at 23 ºC for 5 min. To the resulting brown solution was added 20 mL of pentane before it was filtered through a fine porosity fritted funnel. The filter cake was carried through the frit using 4 mL of CH_2Cl_2 and then filtered again through Celite. The resulting filtrate was equally distributed between eight scintillation vials (approximately 0.5 mL of solution each). Each solution was layered with 3.5 mL pentane and stored in the glovebox freezer at –35 ºC for 18 h. These yielded red crystals, which were harvested and washed with pentane. Combined yield: 14 mg, 22 μmol, 37%. Combustion analysis consistently suggested co-contamination with the byproduct [K(Crypt)]OTf, the presence of which was confirmed via ^{1}H and ^{19}F NMR spectroscopy. The very similar solubilities of **FeL$^{\mathbf{OCH2O}}$** and [K(Crypt)]OTf has rendered separation by extraction unsuccessful.

Synthesis of Fe(DMF)L$^{\mathbf{OMe}}$. In the glovebox, **[K(18-crown-6)][FeL$^{\mathbf{OMe}}$]** (1.09 g, 1.10 mmol, 1.0 eq) was dissolved in 15 mL of CH_2Cl_2. In a separate vial, AgOTf (284 mg, 1.11 mmol, 1.01 eq) was suspended in 5 mL of CH_2Cl_2. Both solutions were cooled to near –90 ºC in the glovebox cold well before the [K(18-crown-6)][FeL^{OMe}] was slowly added to the AgOTf. The red solution was stirred for 15 min while maintaining the temperature near the freezing point of the solvent, and then filtered through a medium porosity fritted funnel topped with Celite. The filtrate was dried *in vacuo* before being redissolved in 30 mL of DMF. The pearlescent solution was filtered through a fine porosity fritted funnel, and the filtrate was divided between two different flasks. The DMF solutions were layered with Et_2O (ratio of 7:1 Et_2O/DMF) and stored at –35 ºC in the glovebox freezer. After two days, red needles were harvested and washed with thawing Et_2O to remove residual DMF. These crystals were dried *in vacuo* to yield **Fe(DMF)L$^{\mathbf{OMe}}$**. Yield: 575 mg, 0.76 mmol, 69%. $\mu_{eff} = 6.4\ \mu_B$ (Evans method, ^{19}F NMR, MeCN/$PhCF_3$, 23 ºC). Material that produced a satisfactory elemental analysis was doubly recrystallized. Calculated combustion analysis for $C_{36}H_{46}FeN_5O_{10}$: C, 56.55%; H, 6.06%; N, 9.16%. Found: C, 56.44%; H, 6.29%; N, 9.20%. Crystals suitable for X-ray diffraction were grown from a concentrated DCM solution layered with Et_2O at –35 ºC.

Synthesis of [K(Crypt)][Fe(F)L$^{\mathbf{OCH2O}}$]. In the glovebox, a scintillation vial was charged with FcOTf (16 mg, 48 μmol, 1.0 eq) and 1 mL of CH_2Cl_2. The solution was added to a scintillation vial containing solid [K(Crypt)][FeL^{OCH2O}] (50.0 mg, 47.2 μmol, 1.0 eq) and a stir bar, and stirred at 23 ºC for 5 min. To the resulting brown solution was added 20 mL of pentane before it was filtered through a fine porosity fritted funnel. The dried filter cake was then added to a scintillation vial containing KF (3.0 mg, 52 μmol, 1.1 eq), [2.2.2.]cryptand (19.5 mg, 52 μmol, 1.1 eq), a stir bar, and 2 mL of MeCN. The solution was stirred at 23 ºC for 1 hour and was filtered through Celite before being concentrated to ~0.5 mL. Diffusing in Et_2O vapor produced yellow crystals suitable for X-ray diffraction. The crystals were washed with Et_2O and dried *in vacuo*. Yield: 10.1 mg, 9.4 μmol, 20%. $\mu_{eff} = 5.95\ \mu_B$ (Evans method, ^{19}F NMR, MeCN/$PhCF_3$, 23 °C). Calculated combustion analysis for $C_{48}H_{63}N_6O_{15}FFeK$: C, 53.48%; H, 5.89%; N, 7.80%. Found: C, 54.17%; H, 5.92%; N, 7.72%.

Synthesis of TBA[Fe(F)L$^{\mathbf{OMe}}$]. In the glovebox, a scintillation vial was charged with **Fe(DMF)L$^{\mathbf{OMe}}$** (50.0 mg, 65.4 μmol, 1.0 eq), tetrabutylammonium fluoride (TBAF; 18 mg, 69 μmol, 1.0 eq), and 2 mL THF. The reaction was stirred at ambient temperature for 1 hr. The yellow solution was filtered through Celite and precipitated by addition of 20 mL Et_2O. The resulting yellow solid was dried in vacuo to yield **TBA[Fe(F)L$^{\mathbf{OMe}}$]**. Yield: 30 mg, 0.032 mmol, 48%. $\mu_{eff} = 5.72\ \mu_B$ (Evans method, ^{19}F NMR, THF/$PhCF_3$, 23 °C). Calculated elemental analysis for $C_{49}H_{75}FFeN_5O_9$: C, 61.76%; H, 7.93%; N, 7.35%. Found: C, 60.97%; H, 8.26%; N, 7.26%. Single crystals suitable for X-ray diffraction were grown by dissolving the product in CH_2Cl_2 and allowing for diffusion of Et_2O vapor in the glovebox.

S3. Additional Electrochemical Data

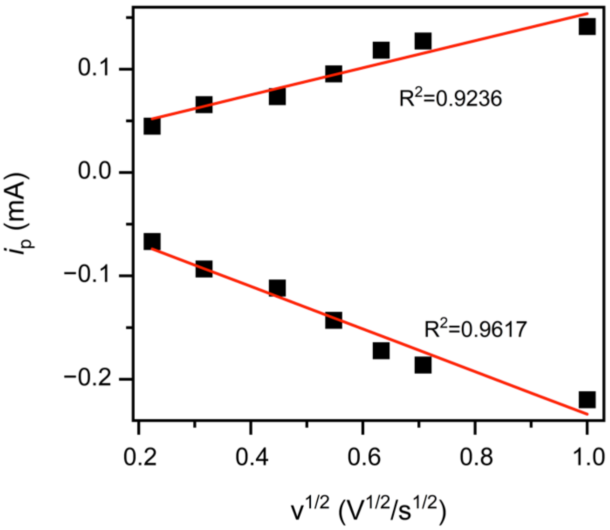

Figure S1. Peak current versus square root of the scan rate of 10 mM **[K(Crypt)][FeL$^{\mathbf{OCH2O}}$]** in anhydrous DMF with 0.1 M [(nBu)$_4$N]PF$_6$ as electrolyte.

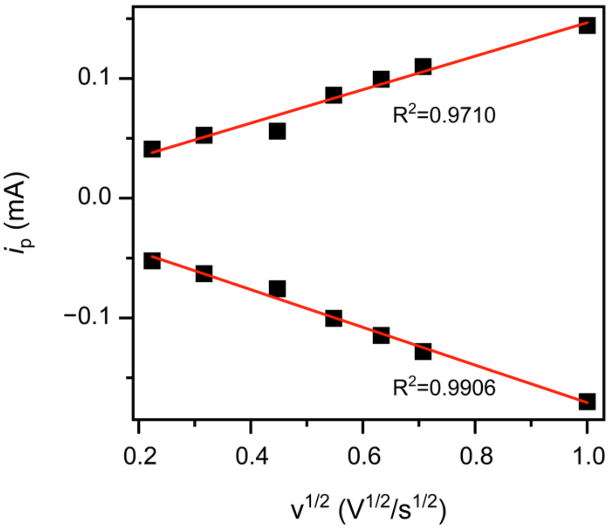

Figure S2. Peak current versus square root of the scan rate of 10 mM **[K(18-crown-6)][FeL$^{\mathbf{OMe}}$]** in anhydrous DMF with 0.1 M [(nBu)$_4$N]PF$_6$ as electrolyte.

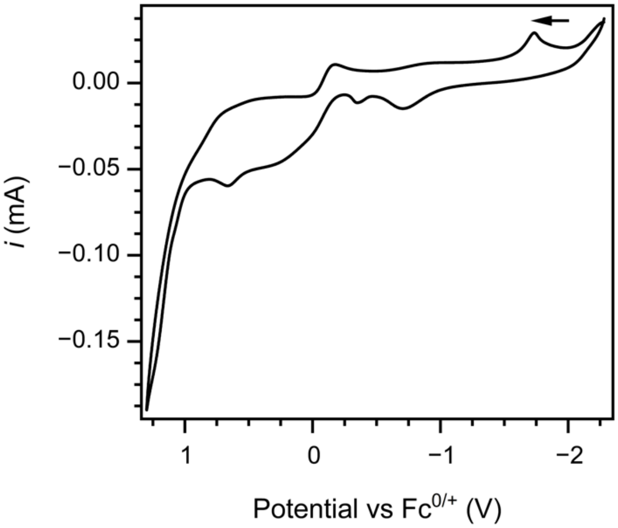

Figure S3. Voltammogram of **[K(Crypt)][FeL$^{\mathbf{OCH2O}}$]** scanning across the entire DMF solvent window. A freshly polished glassy carbon working electrode was used. Two identical scans were performed immediately preceding that shown here. Conditions: 0.1 V/s; 10 mM analyte; 0.1 M $[(n\text{Bu})_4\text{N}]\text{PF}_6$; anhydrous DMF solvent; ambient temperature; N_2 atmosphere. Arrow denotes sweep direction.

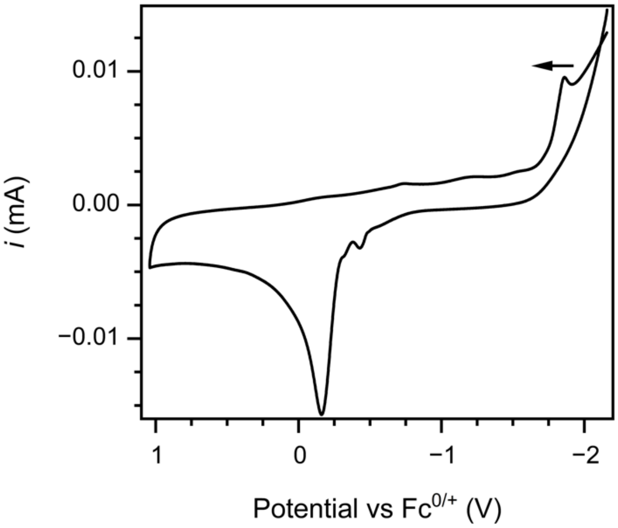

Figure S4. Voltammogram of **[K(Crypt)][FeL$^{\mathbf{OCH2O}}$]** scanning across the entire CH_2Cl_2 solvent window. A freshly polished glassy carbon working electrode was used. Two identical scans were performed immediately preceding that shown here. Conditions: 0.1 V/s; 1 mM analyte; 0.1 M $[(n\text{Bu})_4\text{N}]\text{PF}_6$; anhydrous CH_2Cl_2 solvent; ambient temperature; N_2 atmosphere. Arrow denotes sweep direction.

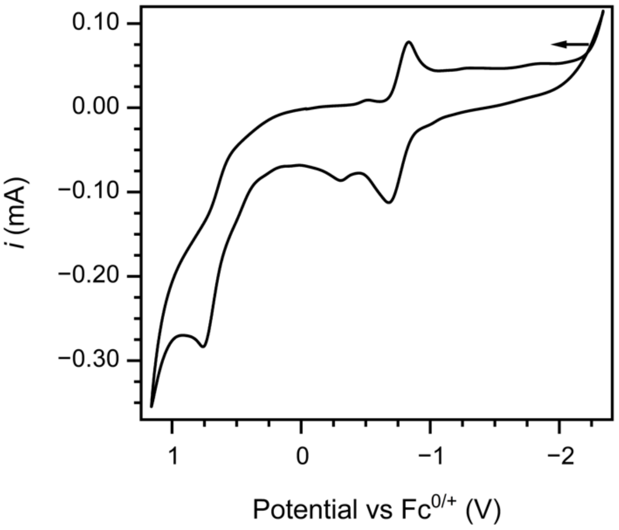

Figure S5. Voltammogram of **[K(18-crown-6)][FeL^{OMe}]** scanning across the entire DMF solvent window. A freshly polished glassy carbon working electrode was used. Two identical scans were performed immediately preceding that shown here. Conditions: 1 V/s; 10 mM analyte; 0.1 M [(nBu)$_4$N]PF$_6$; anhydrous DMF solvent; ambient temperature; N$_2$ atmosphere. Arrow denotes sweep direction.

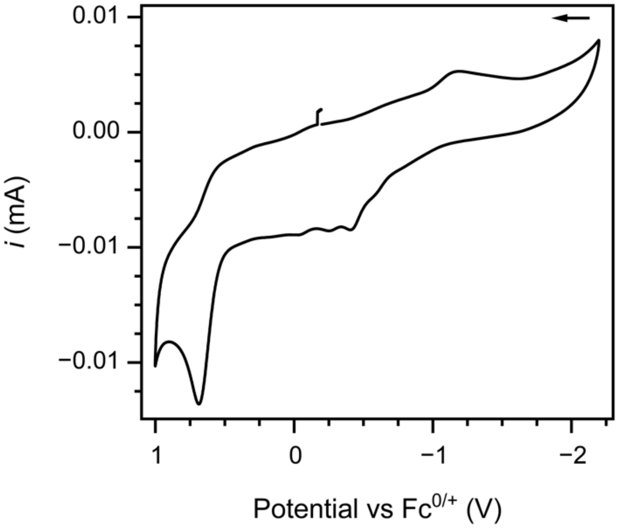

Figure S6. Voltammogram of **[K(18-crown-6)][FeL^{OMe}]** scanning across the entire CH_2Cl_2 solvent window. A freshly polished glassy carbon working electrode was used. Two identical scans were performed immediately preceding that shown here. Conditions: 0.1 V/s; 1 mM analyte; 0.1 M [(nBu)$_4$N]PF$_6$; anhydrous CH_2Cl_2 solvent; ambient temperature; N$_2$ atmosphere. Arrow denotes sweep direction.

S4. Additional Electronic Spectroscopy Data.

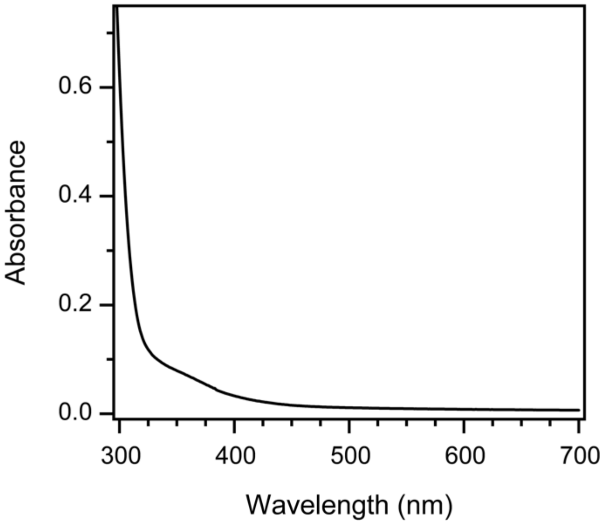

Figure S7. Electronic spectrum of 0.1 mM **[K(18-crown-6)][FeL^{OMe}]** in DMF at 23 ºC.

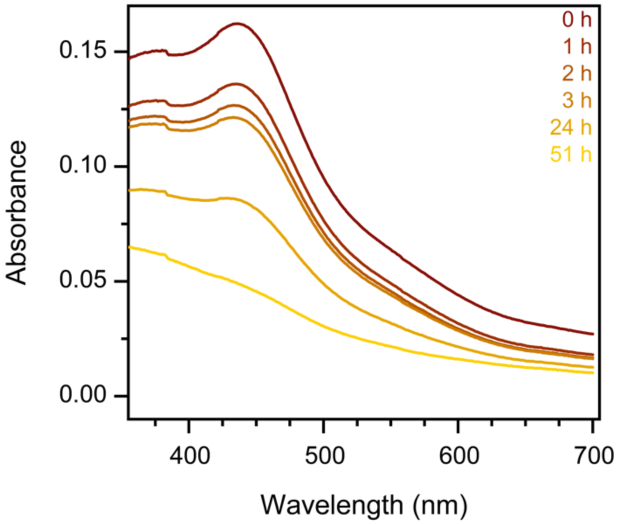

Figure S8. Electronic spectra of **FeL^{OCH2O}** in CH_2Cl_2 at 23 ºC.

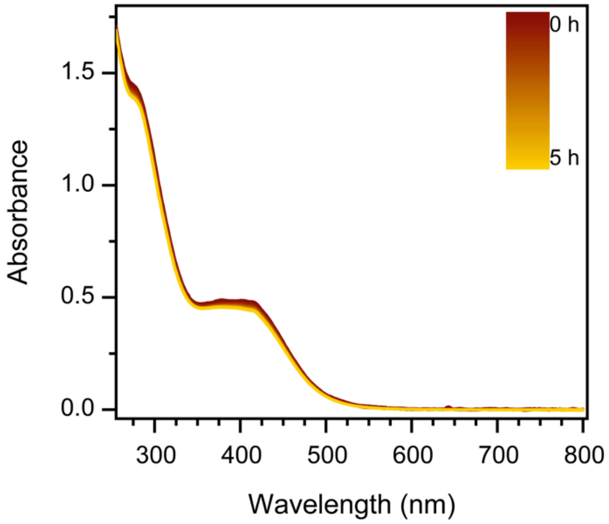

Figure S9. Electronic spectra of 0.1 mM **Fe(DMF)L$^{\mathbf{OMe}}$** decay in DCM over the course of 5 hours at 23 ºC. Each trace represents one minute.

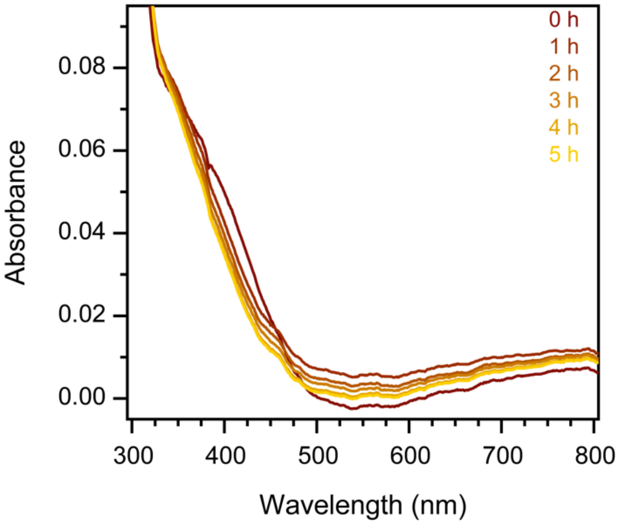

Figure S10. Electronic spectra of the crude reaction mixture resulting from the oxidation of **[FeL$^{\mathbf{OMe}}$]**$^-$ with AgOTf in CH_2Cl_2 prior to any exposure to DMF. Spectra were acquired at 0.3 M at 23 ºC in DCM.

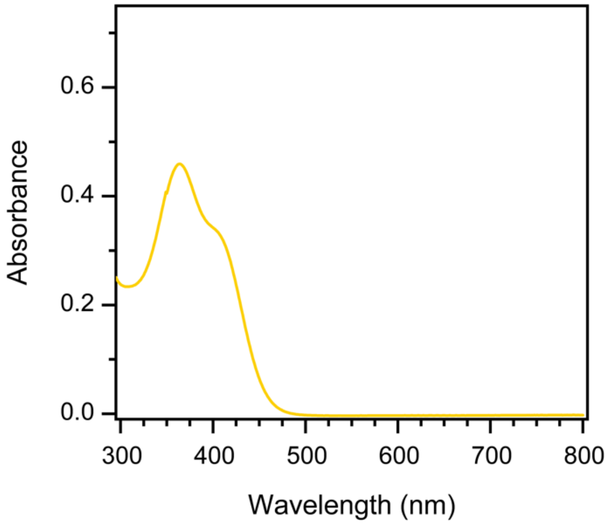

Figure S11. Electronic spectrum of 0.08 mM **[K(Crypt)][Fe(F)L$^{\mathbf{OCH2O}}$]** in MeCN at 23 ºC. At λ_{max} = 364 nm, the ε = 5424 M^{-1} cm^{-1}.

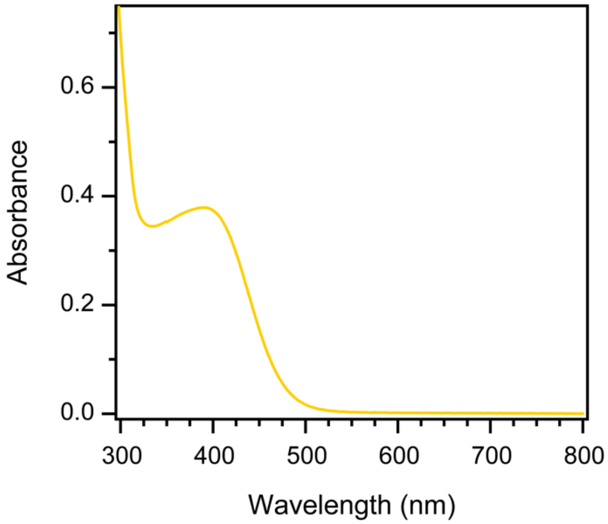

Figure S12. Electronic spectrum of 0.1 mM **TBA[Fe(F)L$^{\mathbf{OMe}}$]** in THF at 23 ºC. At λ_{max} = 388 nm, the ε = 3800 M^{-1} cm^{-1}.

S5. Details of Molecular Dynamics Simulations

Molecular dynamics simulations using quantum mechanical interactions were carried out using the ORCA computational software suite.[6] The pure DFT functional OLYP was found to give computationally tractable results while providing geometries that remain chemically reasonable. OLYP is a Generalized Gradient Approximation (GGA) functional which utilizes OPTX GGA exchange and LYP GGA correlation.[7] This functional has been previously utilized to quantitatively assess the energy surface associated with axial nitrile approach in the related high-spin cobalt(II) complex **[CoL$^{\mathbf{OCH2O}}$]**$^{-}$. All calculations included the D3 dispersion correction.[8] The Alhrichs all-electron triple-zeta basis set def2-TZVP(-f)[9] was employed for Fe, while light atoms were assigned the single-valence basis set def2-SVP.[9] All atoms were assigned the def2/J auxiliary basis set.[10] Prior to simulations, the gas-phase geometry of each analyzed structure was relaxed. Spin-unrestricted geometry optimizations utilized the TIGHTOPT and TIGHTSCF criteria. In accordance with experimental findings, the high-spin electronic state (S = 2 for ferrous complexes; S = 5/2 for **FeL$^{\mathbf{OCH2O}}$**) was confirmed to be the lowest-energy configuration by comparing the energies of the relaxed geometries for all possible electronic states.

The NVT molecular dynamics simulations were run for a total of 1500 fs at 298 K. The "NormalSCF" convergence tolerance (1.0e-06) and the CSVR thermostat were used. The timestep for the simulations was 1 fs and the trajectories were saved every 10 fs (energy and temperature data were saved for every step/1 fs). All simulations were run with both a 10 fs and a 50 fs CSVR time constant. Both time constants give quantitatively very similar results. Unless specified below, all data shown correspond to 50 fs CSVR time constant simulations.

As described in the main text, special attention was paid to two geometric parameters, as they report on regions of space through which an exogenous reactant could conceivably access the unsaturated metal center. The first is the aperture width at the cavity rim, approximated as the mean distance between the *para* H atoms on the aryl rings after subtracting out the van der Waals radii of each H atom (1.2 Å).[11] While the quantitative fidelity of this metric as a reporter on the effective aperture width is unknown, comparisons across different complexes should allow us to determine whether qualitative differences exist as a function of oxidation state and/or metal identity. Figure S13 depicts the relevant H atoms at the rim of the cavity.

Figure S14 displays the aperture width as defined above for **[FeL$^{\mathbf{OCH2O}}$]$^{\mathbf{n}}$** (n = 0, –1) during the course of our simulations. We again note that the quantitative values should be interpreted with caution; however, the highly similar results seen for both complexes suggest that the valence state of iron has a minimal impact on dynamics at the cavity rim.

The second group of parameters analyzed through MD simulations are the N_{eq}–Fe–N_{eq} angles present in each complex. As these angles flex to larger values (beyond their equilibrium values of approximately 115–125°), they expose a greater portion of the ligated metal center to the exterior environment. The quantitatively similar results seen for **[FeL$^{\mathbf{OCH2O}}$]$^{\mathbf{n}}$** (n = 0, –1) and **[FeL$^{\mathbf{OMe}}$]**$^{-}$ (Figures 4 and S15–18) suggests that flexibility within the primary coordination sphere is minimally affected by the presence (or absence) of a rigid macrocycle in the secondary coordination sphere.

As seen in Figures S19, S22, and S25 the systems all appear to have reached thermal equilibrium by approximately 300 fs. The kinetic energy (Figures S21, S24, S27) and temperature (Figures S19, S22, S25) behavior are very similar, which is expected as the instantaneous kinetic energy and the calculated temperature are directly related. There are no qualitative differences seen in the relevant metrical parameters (*e.g.* aperture width, N–Fe–N angles) before and after thermal equilibrium has been reached.

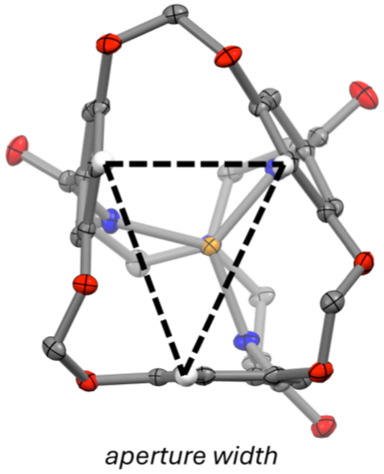

Figure S13. Depiction of how "aperture width" is defined for simulations involving **[FeL$^{\mathbf{OCH2O}}$]$^{\mathbf{n}}$** (n = 0, –1). The mean distance between *para* H atoms, minus the van der Waals radii of each H atom, is hypothesized to report on the effective aperture width. All other hydrogen atoms have been omitted for clarity.

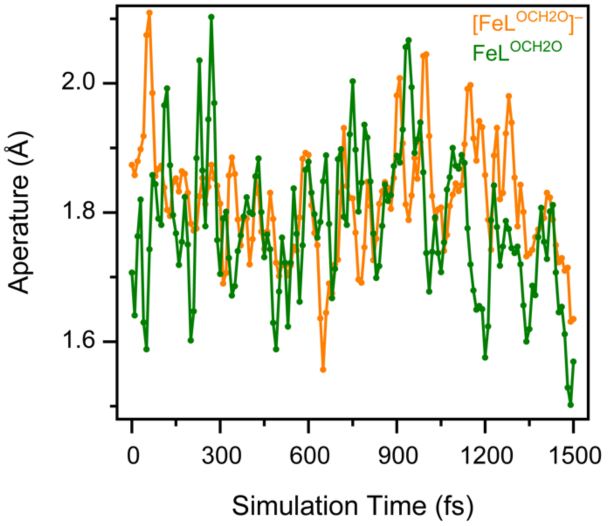

Figure S14. Calculated aperture widths for **[FeL$^{\mathbf{OCH2O}}$]$^{\mathbf{n}}$** (n = 0, –1).

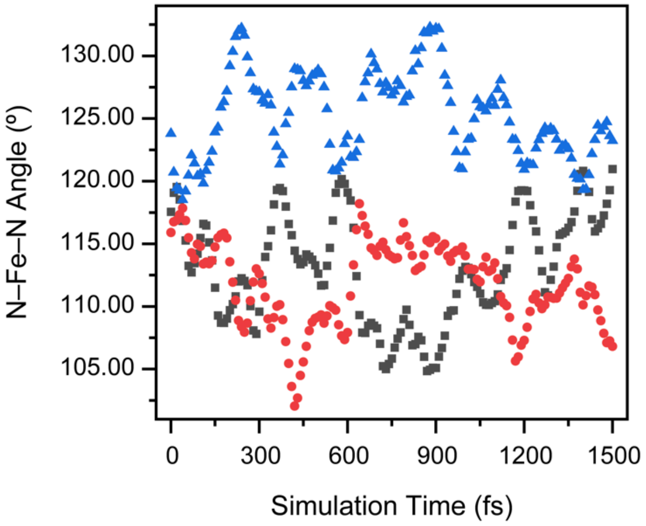

Figure S15. Equatorial N–Fe–N angles for **FeL$^{\mathbf{OCH2O}}$** with 50 fs CSVR time constant. The colors represent the arbitrary assignment of the three possible N–Fe–N angles.

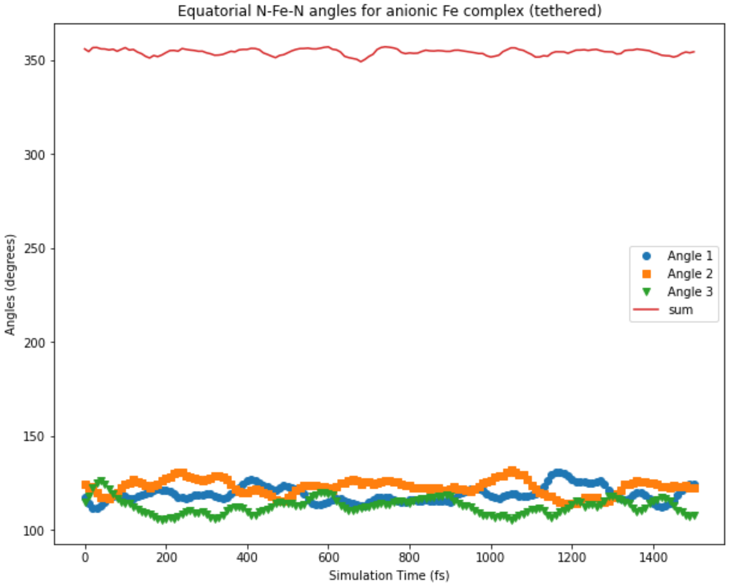

Figure S16. Equatorial N–Fe–N angles for **[FeL$^{\mathbf{OCH2O}}$]$^{-}$**.

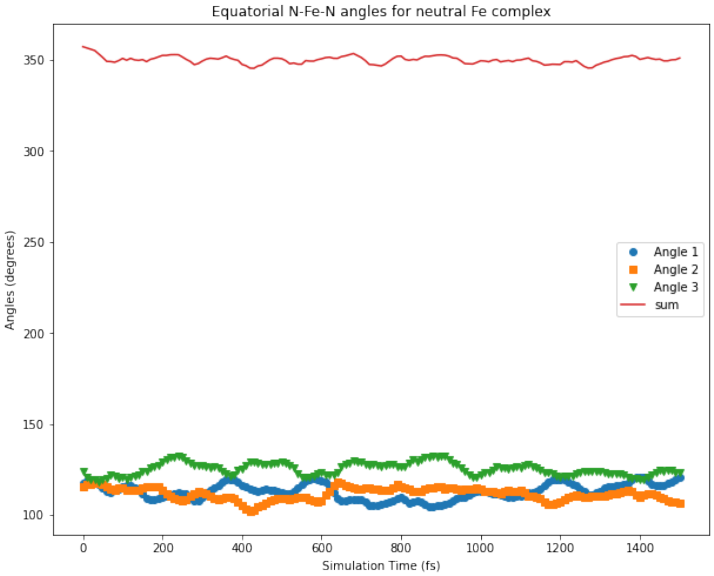

Figure S17. Equatorial N–Fe–N angles for **FeL$^{\mathbf{OCH2O}}$**.

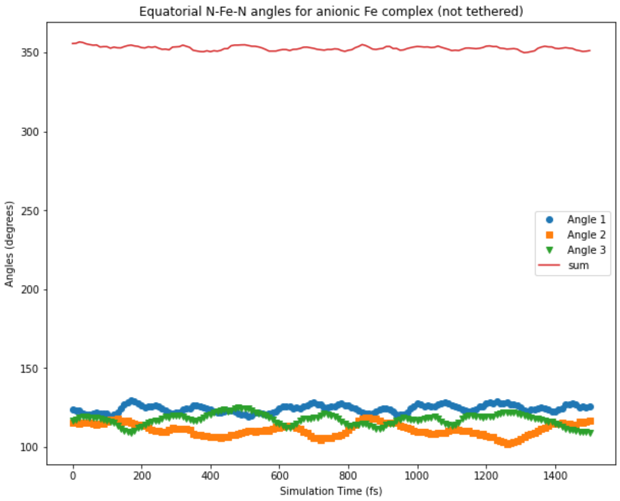

Figure S18. Equatorial N–Fe–N angles for **[FeL$^{\mathbf{OMe}}$]$^{-}$**.

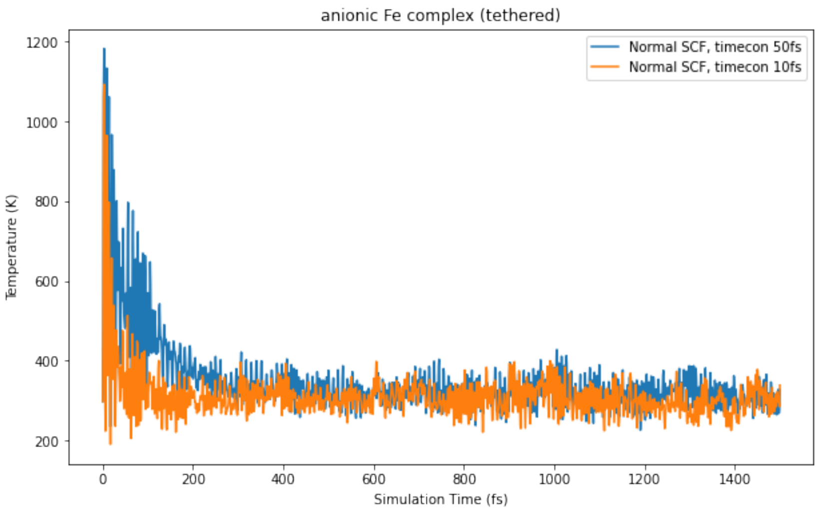

Figure S19. Temperature as a function of simulation time for **[FeL$^{\mathbf{OCH2O}}$]$^{-}$**.

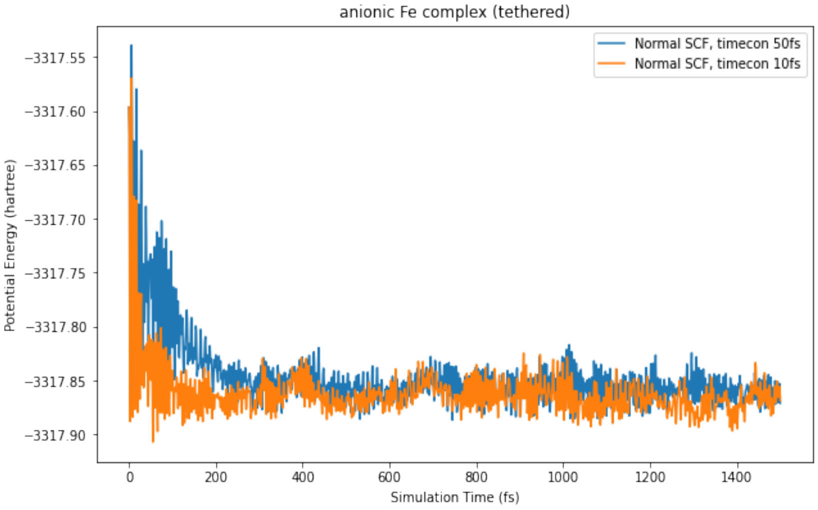

Figure S20. Potential energy as a function of simulation time for **[FeL$^{\mathbf{OCH2O}}$]$^{-}$**.

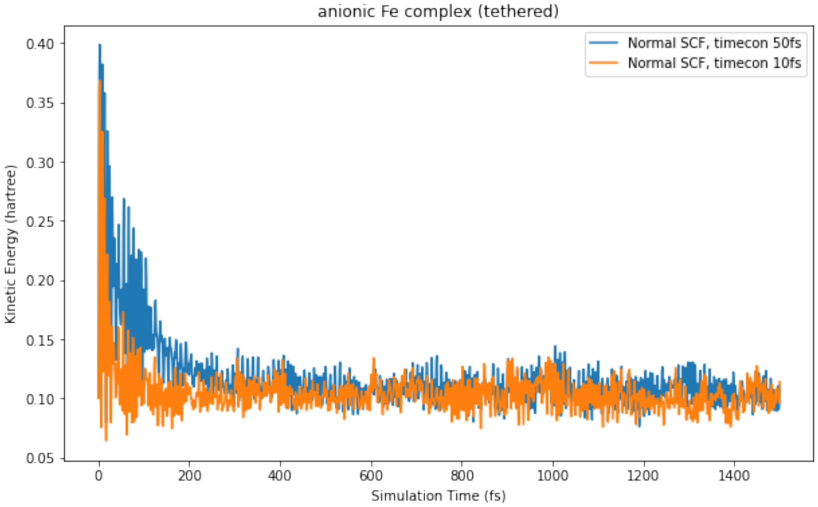

Figure S21. Kinetic energy as a function of simulation time for **[FeL$^{\mathbf{OCH2O}}$]$^{-}$**.

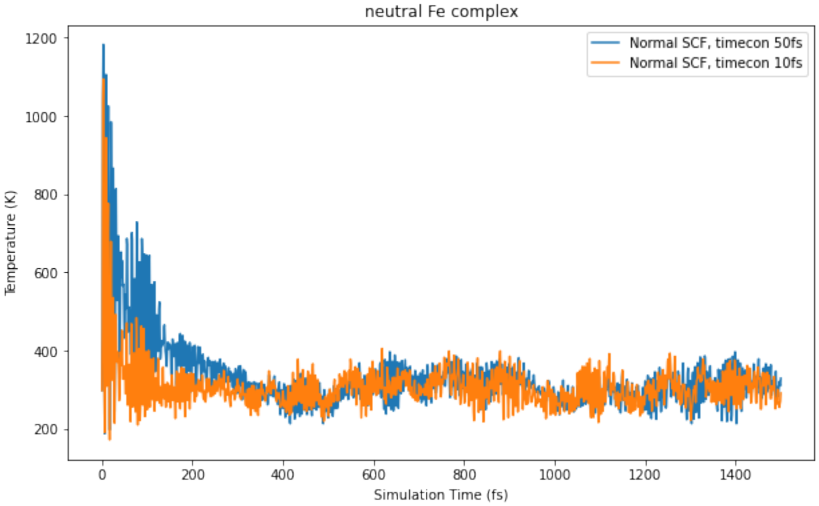

Figure S22. Temperature as a function of simulation time for **FeL$^{\mathbf{OCH2O}}$**.

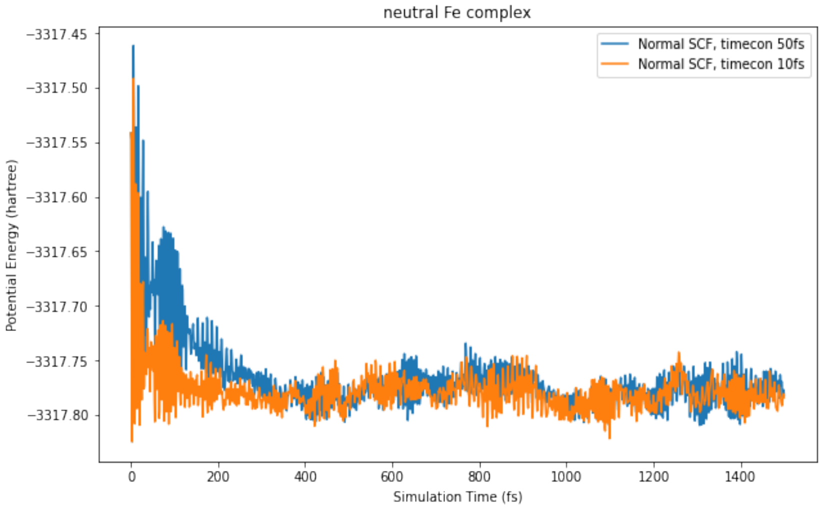

Figure S23. Potential energy as a function of simulation time for **FeL$^{\mathbf{OCH2O}}$**.

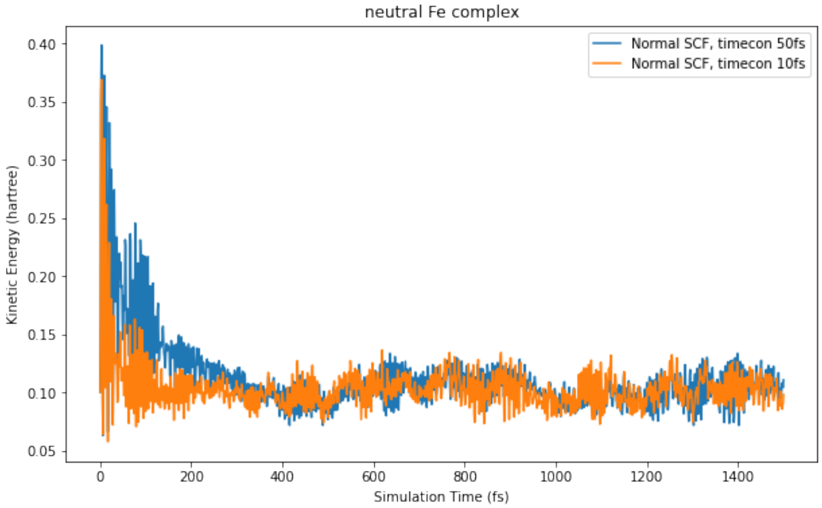

Figure S24. Kinetic energy as a function of simulation time for **FeL$^{\mathbf{OCH2O}}$**.

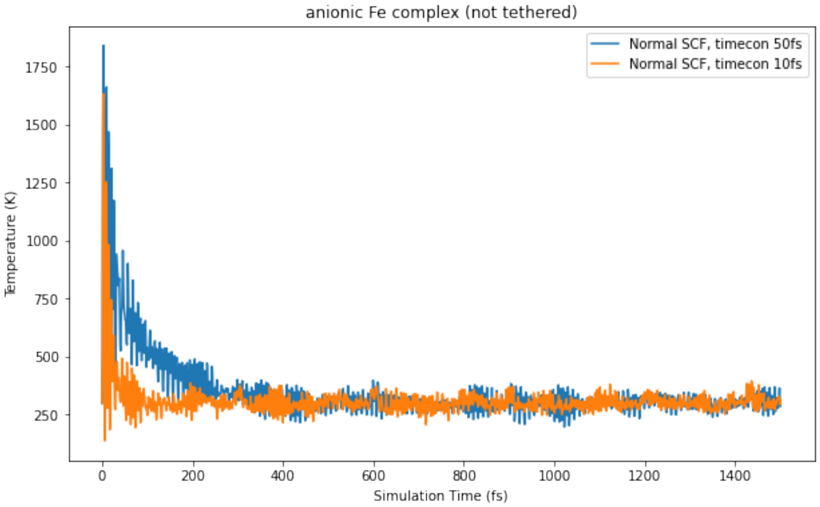

Figure S25. Temperature as a function of simulation time for **[FeL$^{\mathbf{OMe}}$]$^{-}$**.

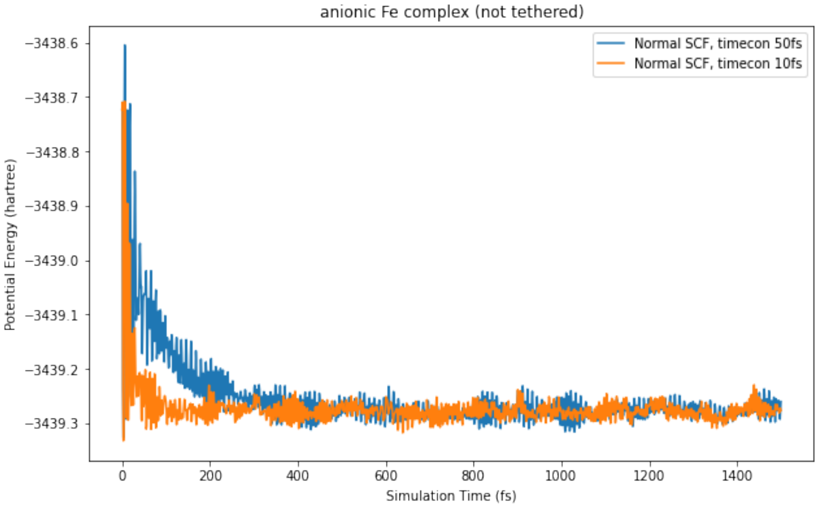

Figure S26. Potential energy as a function of simulation time for **[FeL$^{\mathbf{OMe}}$]$^{-}$**.

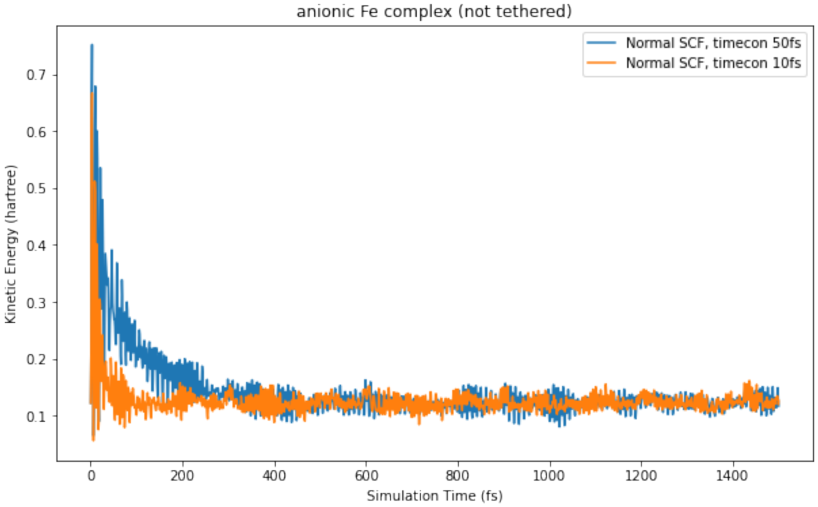

Figure S27. Kinetic energy as a function of simulation time for **[FeL^{OMe}]$^-$**.

S6. Electron Paramagnetic Resonance Data.

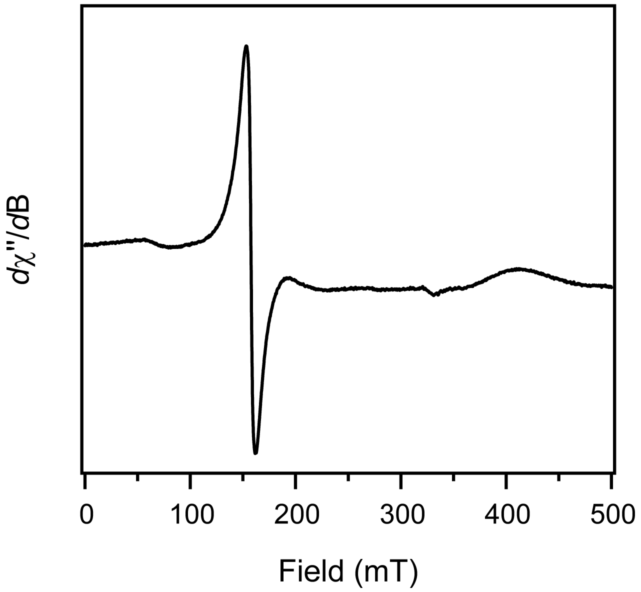

Figure S28. X-band EPR spectrum obtained by dissolving a sample of **FeL^{OCH2O}** in CH_2Cl_2, glassing in liquid nitrogen, and cooling to 10 K in the spectrometer for analysis. The predominant feature at $g = 4.3$ is believed to arise from an impurity or decomposition product, rather than to reflect a signal originating from **FeL^{OCH2O}**.

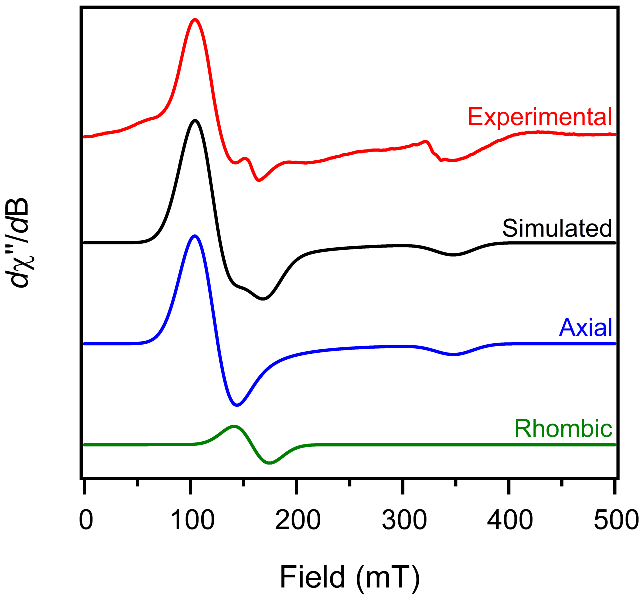

Figure S29. Comparison of experimental and simulated X-band EPR spectra for **Fe(DMF)L$^{\mathbf{OMe}}$** in glassed MeCN solution at 10 K. The simulation is a sum of axial (g = [5.86, 1.92], lwpp = 35.0 mT; 92%) and rhombic (g_{iso} = 4.25, lwpp = 33.4 mT, 8%) components.

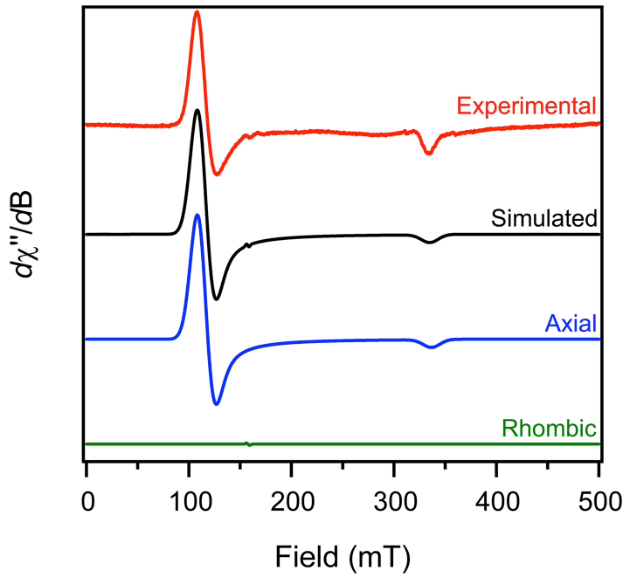

Figure S30. Comparison of experimental and simulated X-band EPR spectra for **[K(Crypt)][Fe(F)L$^{\mathbf{OCH2O}}$]** in glassed CH_2Cl_2 solution at 10 K. The simulation is a sum of axial (g = [5.94, 2.00], lwpp = 16.2 mT; 99.99%) and rhombic (g_{iso} = 4.26, lwpp = 2.7 mT, 0.01%) components.

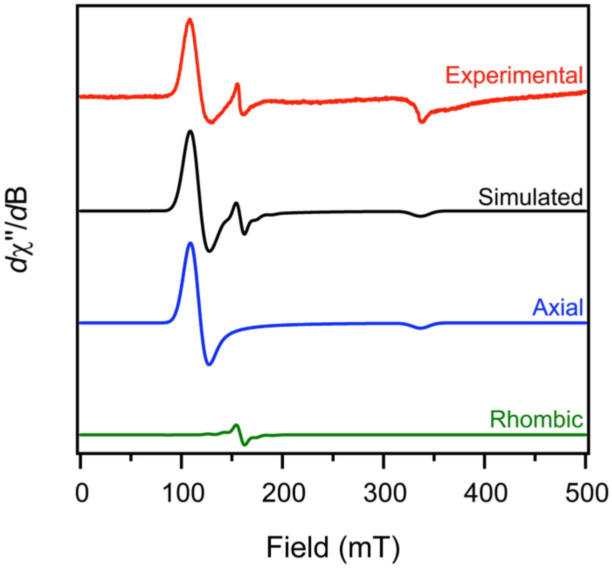

Figure S31. Comparison of experimental and simulated X-band EPR spectra for **TBA[Fe(F)L^{OMe}]** in glassed CH_2Cl_2 solution at 10 K. The simulation is a sum of axial (g = [5.91, 1.99], lwpp = 16.4 mT; 96%) and rhombic (g_{iso} = 4.25, lwpp = 7.8 mT, 4%) components.

S7. Details of Crystallographic Structure Determinations

S7.1. CCDC Deposition. All five crystal structures reported herein have been deposited with the Cambridge Crystallographic Data Center (CCDC) and have been assigned the CCDC deposition numbers 2422256-2422260.

S7.2. Details of data collection, structure solution, and refinement.

FeL^{OCH2O} • CH_2Cl_2. A crystal (0.179 x 0.079 x 0.06 mm^3) was placed onto a thin glass optical fiber or a nylon loop and mounted on a Rigaku XtaLAB Synergy-S Dualflex diffractometer equipped with a HyPix-6000HE HPC area detector for data collection at 100.00(10) K. A preliminary set of cell constants and an orientation matrix were calculated from a small sampling of reflections.[12] A short pre-experiment was run, from which an optimal data collection strategy was determined. The full data collection was carried out using a PhotonJet (Cu) X-ray source with frame times of 0.50 and 2.00 seconds and a detector distance of 34.0 mm. Series of frames were collected in 0.50° steps in ω at different 2θ, κ, and ϕ settings. After the intensity data were corrected for absorption, the final cell constants were calculated from the xyz centroids of 31857 strong reflections from the actual data collection after integration.[12] See Table S2 for additional crystal and refinement information.

The structure was solved using SHELXT[13] and refined using SHELXL.[14] The space group $P2_1/n$ was determined based on systematic absences. Most or all non-hydrogen atoms were assigned from the solution. Full-matrix least squares / difference Fourier cycles were performed which located any remaining non-hydrogen atoms. All non-hydrogen atoms were refined with anisotropic displacement parameters. All hydrogen atoms were placed in ideal positions and refined as riding atoms with relative isotropic displacement parameters. The final full matrix least squares refinement converged to $R1 = 0.0347$ (F^2, $I > 2\sigma(I)$) and $wR2 = 0.0950$ (F^2, all data). Structure manipulation and figure generation were performed within the Olex2 program.[15]

The structure is the one suggested. The asymmetric unit contains one iron complex and one dichloromethane solvent molecule of crystallization in general positions. The N-CH2-CH2-N linkages are modeled as disordered over two positions (0.75:0.25).

[K(18-crown-6)][FeL$^{\mathbf{OMe}}$]. A crystal (0.22 x 0.148 x 0.053 mm^3) was placed onto a thin glass optical fiber or a nylon loop and mounted on a Rigaku XtaLAB Synergy-S Dualflex diffractometer equipped with a HyPix-6000HE HPC area detector for data collection at 100.00(10) K. A preliminary set of cell constants and an orientation matrix were calculated from a small sampling of reflections.[12] A short pre-experiment was run, from which an optimal data collection strategy was determined. The full data collection was carried out using a PhotonJet (Cu) X-ray source with frame times of 0.35 and 1.41 seconds and a detector distance of 34.0 mm. Series of frames were collected in 0.50° steps in ω at different 2θ, κ, and ϕ settings. After the intensity data were corrected for absorption, the final cell constants were calculated from the xyz centroids of 43543 strong reflections from the actual data collection after integration.[12] See Table S3 for additional crystal and refinement information.

The structure was solved using SHELXT[13] and refined using SHELXL.[14] The space group $P2_1/c$ was determined based on systematic absences. Most or all non-hydrogen atoms were assigned from the solution. Full-matrix least squares / difference Fourier cycles were performed which located any remaining non-hydrogen atoms. All non-hydrogen atoms were refined with anisotropic displacement parameters. All hydrogen atoms were placed in ideal positions and refined as riding atoms with relative isotropic displacement parameters. The final full matrix least squares refinement converged to $R1 = 0.0349$ (F^2, $I > 2\sigma(I)$) and $wR2 = 0.0932$ (F^2, all data). Structure manipulation and figure generation were performed within the Olex2 program.[15]

The asymmetric unit contains one cation-anion pairing in a general position. One segment of the crown ether, O13-O15, is modeled as disordered over two positions (0.77:0.23). The alternating cations and anions are linked one-dimensionally via K…O contacts.

Fe(DMF)L$^{\mathbf{OMe}}$ • 3 $\mathbf{CH_2Cl_2}$. A crystal (0.074 x 0.068 x 0.049 mm^3) was placed onto a nylon mesh and mounted on a Rigaku XtaLAB Synergy-S Dualflex diffractometer equipped with a HyPix-6000HE HPC area detector for data collection at 100.01(10) K. A preliminary set of cell constants and an orientation matrix were calculated from a small sampling of reflections.[12] A short pre-experiment was run, from which an optimal data collection strategy was determined. The full data collection was carried out using a PhotonJet (Cu) X-ray source with frame times of 9.05 and 36.20 seconds and a detector distance of 34.0 mm. Series of frames were collected in 0.50° steps in ω at different 2θ, κ, and ϕ settings. After the intensity data were corrected for absorption, the final cell constants were calculated from the xyz centroids of 14275 strong reflections from the actual data collection after integration.[12] See Table S4 for additional crystal and refinement information.

The structure was solved using SHELXT[13] and refined using SHELXL.[14] The space group $P2_1/n$ was determined based on systematic absences. Most or all non-hydrogen atoms were assigned from the solution. Full-matrix least squares / difference Fourier cycles were performed which located any remaining non-hydrogen atoms. All non-hydrogen atoms were refined with anisotropic displacement parameters. All hydrogen atoms were placed in ideal positions and refined as riding atoms with relative isotropic displacement parameters. The final full matrix least squares refinement converged to $R1 = 0.0534$ (F^2, $I > 2\sigma(I)$) and $wR2 = 0.1450$ (F^2, all data). Structure manipulation and figure generation were performed within the Olex2 program.[15]

The structure is the one suggested. The asymmetric unit contains one iron complex and three dichloromethane solvent molecules of crystallization, all in general positions.

[K(Crypt)][Fe(F)L$^{\mathbf{OCH2O}}$]. A crystal (0.263 x 0.149 x 0.055 mm3) was placed onto a nylon loop and mounted on a Rigaku XtaLAB Synergy-S Dualflex diffractometer equipped with a HyPix-6000HE HPC area detector for data collection at 100.00(10) K. A preliminary set of cell constants and an orientation matrix were calculated from a small sampling of reflections.[12] A short pre-experiment was run, from which an optimal data collection strategy was determined. The full data collection was carried out using a PhotonJet (Mo) X-ray source with a frame time of 47.91 seconds and a detector distance of 34.0 mm. Series of frames were collected in 0.50º steps in ω at different 2θ, κ, and ϕ settings. After the intensity data were corrected for absorption, the final cell constants were calculated from the xyz centroids of 27606 strong reflections from the actual data collection after integration.[12] See Table S5 for additional crystal and refinement information.

The structure was solved using SHELXT[13] and refined using SHELXL.[14] The space group $Pca2_1$ was determined based on systematic absences and intensity statistics. Most or all non-hydrogen atoms were assigned from the solution. Refinement proceeded in an iterative fashion, with each stage including full-matrix least squares cycles, followed by a difference Fourier synthesis, which located any remaining electron density. All non-hydrogen atoms were refined with anisotropic displacement parameters. All hydrogen atoms were placed in ideal positions and refined as riding atoms with relative isotropic displacement parameters. The final full matrix least squares refinement converged to $R1 = 0.0537$ (F^2, $I > 2\sigma(I)$) and $wR2 = 0.1364$ (F^2, all data). Structure manipulation and figure generation were performed within the Olex2 program.[15]

The structure is the one suggested. The asymmetric unit contains one monoanionic iron complex and one cryptand-222 potassium cation in general positions. The cation is modeled as disordered over two positions (0.59:0.41) as an approximation for disorder over multiple positions.

TBA[Fe(F)L$^{\mathbf{OMe}}$]. A crystal (0.5 x 0.061 x 0.019 mm^3) was placed onto a nylon loop and mounted on a Rigaku XtaLAB Synergy-S Dualflex diffractometer equipped with a HyPix-6000HE HPC area detector for data collection at 100.00(11) K. A preliminary set of cell constants and an orientation matrix were calculated from a small sampling of reflections.[12] A short pre-experiment was run, from which an optimal data collection strategy was determined. The full data collection was carried out using a PhotonJet (Cu) X-ray source with frame times of 16.00 and 32.00 seconds and a detector distance of 34.0 mm. Series of frames were collected in 0.50º steps in ω at different 2θ, κ, and ϕ settings. After the intensity data were corrected for absorption, the final cell constants were calculated from the xyz centroids of 16979 strong reflections from the actual data collection after integration.[12] See Table S6 for additional crystal and refinement information.

The structure was solved using SHELXT[13] and refined using SHELXL.[14] The space group $P2_1/c$ was determined based on systematic absences. Most or all non-hydrogen atoms were assigned from the solution. Refinement proceeded in an iterative fashion, with each stage including full-matrix least squares cycles, followed by a difference Fourier synthesis, which located any remaining electron density. All non-hydrogen atoms were refined with anisotropic displacement parameters. All hydrogen atoms were placed in ideal positions and refined as riding atoms with relative isotropic displacement parameters. The final full matrix least squares refinement converged to $R1 = 0.0514$ (F^2, $I > 2\sigma(I)$) and $wR2 = 0.1406$ (F^2, all data). Structure manipulation and figure generation were performed within the Olex2 program.[15]

The structure is the one suggested. The asymmetric unit contains two tetrabutylammonium cations and two monoanionic iron complexes in general positions. Methoxy groups O5-C15 and O15-C48 are modeled as disordered over two positions each (0.59:0.41 and 0.61:0.39, respectively). Dimethoxyphenyl group C59-C64/O17-C65/O18-C66 is modeled as disordered over two positions (0.72:0.28). Alkyl chains C75-C78 and C79-C82 are modeled as disordered over two positions each (0.75:0.25 and 0.63:0.37, respectively). Tetrabutylammonium cation N2/C83-C98 is modeled as disordered over two positions (0.72:0.28). Iron atoms Fe1 and Fe2 are out of the N2-N3-N4 and N6-N7-N8 planes, away from atoms N1 and N5, by 0.4113(13) and 0.3915(12) Å, respectively.

Table S1. Selected metrical parameters derived from the solid-state structures of **$[\mathrm{FeL}^{\mathrm{OCH2O}}]^{n}$** (n = 0, –1), **$[\mathrm{FeL}^{\mathrm{OMe}}]^{-}$**, and **$\mathrm{Fe(DMF)L}^{\mathrm{OMe}}$**. Data for **$[\mathrm{FeL}^{\mathrm{OCH2O}}]^{-}$** are taken from Ref. 3.

Complex	Fe–N_{axial} (Å)	Mean Fe–N_{eq} (Å)	Mean N_{eq}–Fe–N_{eq} (°)	Fe–O_{DMF}	Fe Out of Equatorial Plane (Å)
$[\mathrm{FeL}^{\mathrm{OCH2O}}]^{-}$	2.1471(15)	2.033(3)	118.74(14)	n/a	0.2288(9)
$\mathrm{FeL}^{\mathrm{OCH2O}}$	2.0894(15)	1.967(3)	119.09(12)	n/a	0.1886(9)
$[\mathrm{FeL}^{\mathrm{OMe}}]^{-}$	2.2034(13)	2.014(2)	118.58(10)	n/a	0.2417(8)
$\mathrm{Fe(DMF)L}^{\mathrm{OMe}}$	2.290(3)	2.005(3)	116.61(17)	1.985(2)	0.3735(15)

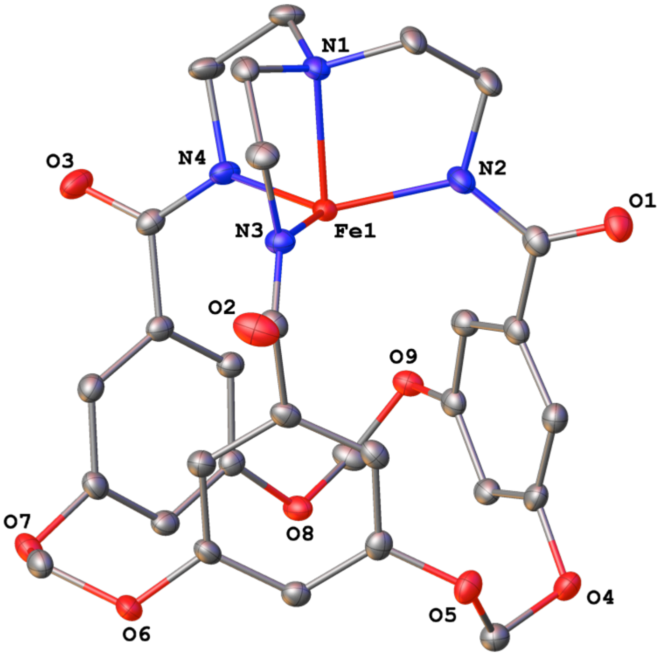

Figure S32. Molecular structure of **FeL$^{\mathbf{OCH2O}}$ • CH$_2$Cl$_2$**. Hydrogen atoms and co-crystallized solvent molecules are omitted for clarity. Anisotropic displacement ellipsoids are drawn at the 50% probability level.

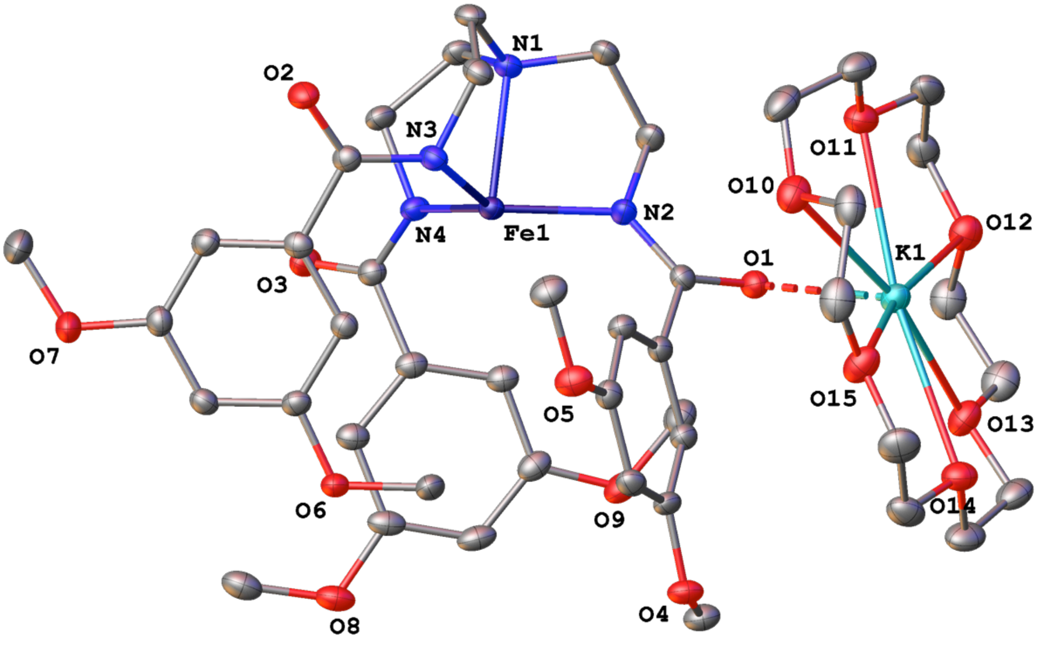

Figure S33. Molecular structure of **[K(18-crown-6][FeL$^{\mathbf{OMe}}$]**. Hydrogen atoms are omitted for clarity. Anisotropic displacement ellipsoids are drawn at the 50% probability level.

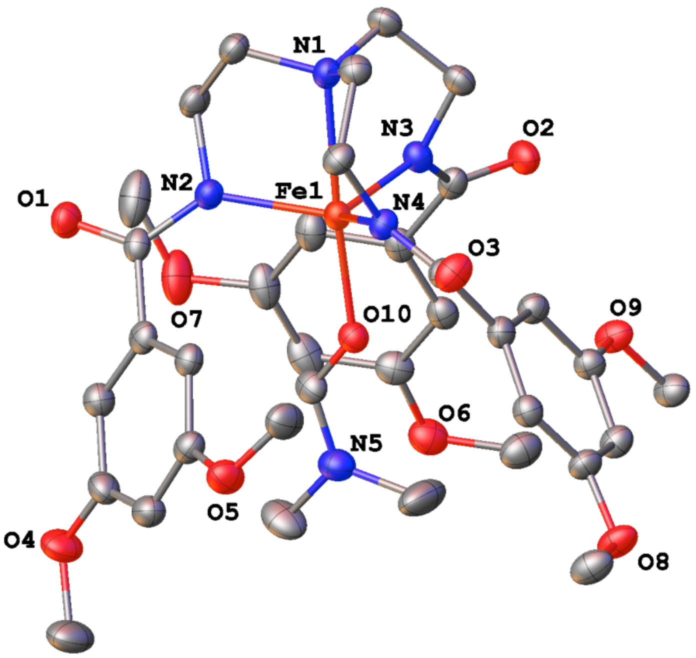

Figure S34. Molecular structure of **Fe(DMF)L^{OMe} • 3 CH$_2$Cl$_2$**. Hydrogen atoms and co-crystallized solvent molecules are omitted for clarity. Anisotropic displacement ellipsoids are drawn at the 50% probability level.

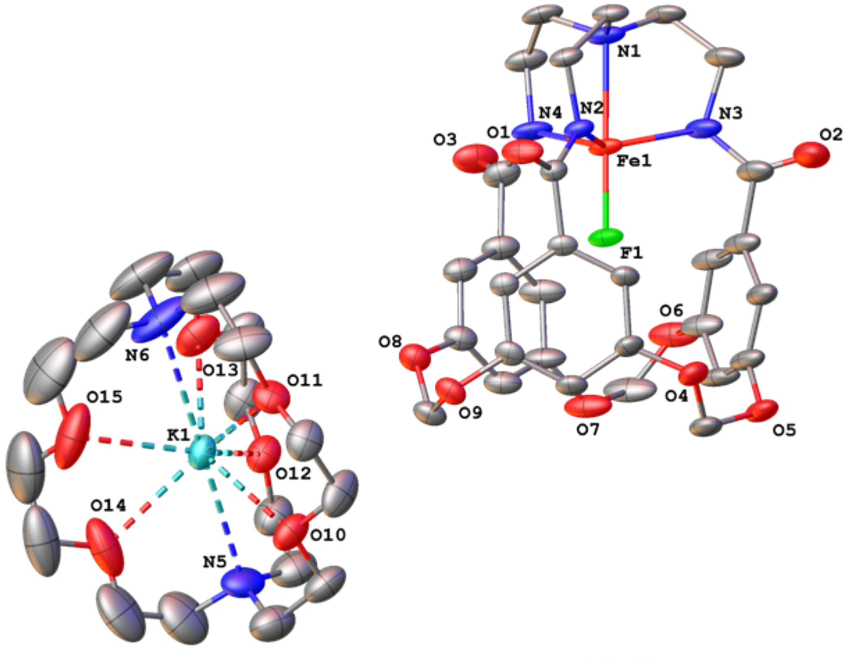

Figure S35. Molecular structure of **[K(Crypt)][Fe(F)L^{OCH2O}]**. Hydrogen atoms and co-crystallized solvent molecules are omitted for clarity. Anisotropic displacement ellipsoids are drawn at the 50% probability level.

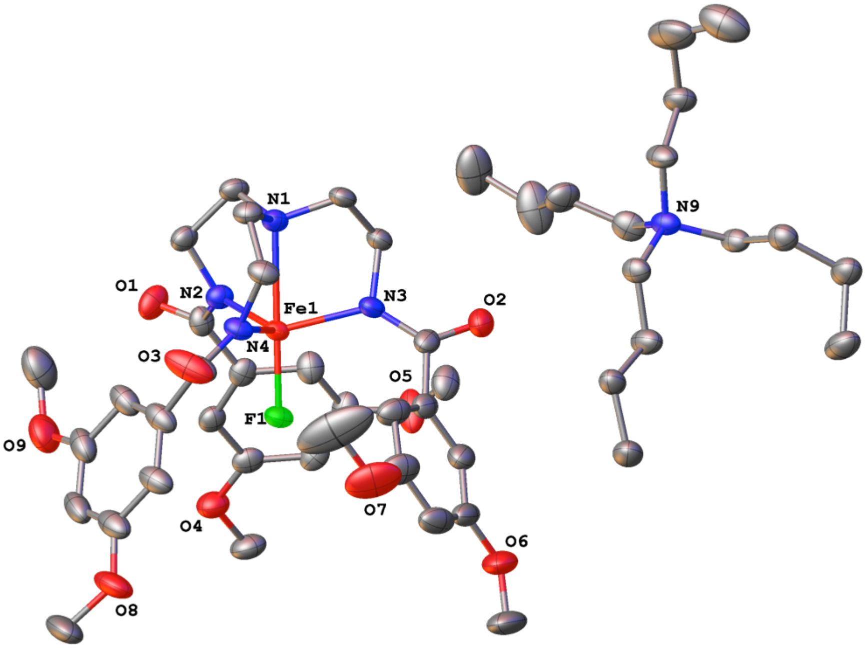

Figure S36. Molecular structure of **TBA[Fe(F)L$^{\mathbf{OMe}}$]**. Hydrogen atoms are omitted for clarity. Anisotropic displacement ellipsoids are drawn at the 50% probability level.

Table S2. Crystal data and structure refinement for **FeL$^{\mathbf{OCH2O}}$**.

Identification code	brbbrb20	
Empirical formula	C31 H29 Cl2 Fe N4 O9	
Formula weight	728.33	
Temperature	100.00(10) K	
Wavelength	1.54184 Å	
Crystal system	monoclinic	
Space group	$P2_1/n$	
Unit cell dimensions	a = 11.80990(10) Å	α = 90°
	b = 15.73550(10) Å	β = 105.3320(10)°
	c = 16.50520(10) Å	γ = 90°
Volume	2958.07(4) Å^3	
Z	4	
Density (calculated)	1.635 Mg/m^3	
Absorption coefficient	6.317 mm^{-1}	
F(000)	1500	
Crystal color, morphology	red, block	
Crystal size	0.179 x 0.079 x 0.06 mm^3	
Theta range for data collection	3.950 to 80.205°	
Index ranges	$-15 \le h \le 14$, $-19 \le k \le 19$, $-21 \le l \le 21$	
Reflections collected	51212	
Independent reflections	6386 [R(int) = 0.0382]	
Observed reflections	6088	
Completeness to theta = 74.504°	100.0%	
Absorption correction	Multi-scan	
Max. and min. transmission	1.00000 and 0.75715	
Refinement method	Full-matrix least-squares on F^2	
Data / restraints / parameters	6386 / 6 / 452	
Goodness-of-fit on F^2	1.067	
Final R indices [I>2sigma(I)]	$R1$ = 0.0347, $wR2$ = 0.0939	
R indices (all data)	$R1$ = 0.0363, $wR2$ = 0.0950	
Largest diff. peak and hole	0.695 and -0.661 e.Å^{-3}	

Table S3. Crystal data and structure refinement for **[K(18-crown-6)][FeL^{OMe}]**.

Identification code	brbcdh15	
Empirical formula	C45 H63 Fe K N4 O15	
Formula weight	994.94	
Temperature	100.00(10) K	
Wavelength	1.54184 Å	
Crystal system	monoclinic	
Space group	$P2_1/c$	
Unit cell dimensions	a = 10.52253(5) Å	α = 90°
	b = 20.51441(12) Å	β = 91.7336(4)°
	c = 21.90377(12) Å	γ = 90°
Volume	4726.06(4) Å^3	
Z	4	
Density (calculated)	1.398 Mg/m^3	
Absorption coefficient	3.956 mm^{-1}	
F(000)	2104	
Crystal color, morphology	colourless, plate	
Crystal size	0.22 x 0.148 x 0.053 mm^3	
Theta range for data collection	4.038 to 80.420°	
Index ranges	$-10 \leq h \leq 13$, $-26 \leq k \leq 26$, $-28 \leq l \leq 27$	
Reflections collected	80553	
Independent reflections	10163 [R(int) = 0.0414]	
Observed reflections	9477	
Completeness to theta = 74.504°	99.7%	
Absorption correction	Multi-scan	
Max. and min. transmission	1.00000 and 0.78061	
Refinement method	Full-matrix least-squares on F^2	
Data / restraints / parameters	10163 / 92 / 665	
Goodness-of-fit on F^2	1.113	
Final R indices [I>2sigma(I)]	$R1$ = 0.0349, $wR2$ = 0.0915	
R indices (all data)	$R1$ = 0.0376, $wR2$ = 0.0932	
Largest diff. peak and hole	0.322 and -0.444 e.Å^{-3}	

Table S4. Crystal data and structure refinement for **Fe(DMF)L$^{\mathbf{OMe}}$**.

Identification code	brblh02	
Empirical formula	C39 H52 Cl6 Fe N5 O10	
Formula weight	1019.40	
Temperature	100.01(10) K	
Wavelength	1.54184 Å	
Crystal system	monoclinic	
Space group	$P2_1/n$	
Unit cell dimensions	a = 12.5162(2) Å	α = 90°
	b = 13.9489(3) Å	β = 95.120(2)°
	c = 26.6627(4) Å	γ = 90°
Volume	4636.39(14) Å^3	
Z	4	
Density (calculated)	1.460 Mg/m^3	
Absorption coefficient	6.288 mm^{-1}	
F(000)	2116	
Crystal color, morphology	orange-red, block	
Crystal size	0.074 x 0.068 x 0.049 mm^3	
Theta range for data collection	3.328 to 80.430°	
Index ranges	$-16 \le h \le 15$, $-16 \le k \le 17$, $-33 \le l \le 25$	
Reflections collected	35514	
Independent reflections	9764 [R(int) = 0.0524]	
Observed reflections	7498	
Completeness to theta = 74.504°	98.6%	
Absorption correction	Multi-scan	
Max. and min. transmission	1.00000 and 0.78545	
Refinement method	Full-matrix least-squares on F^2	
Data / restraints / parameters	9764 / 0 / 558	
Goodness-of-fit on F^2	1.075	
Final R indices [I>2sigma(I)]	$R1$ = 0.0534, $wR2$ = 0.1355	
R indices (all data)	$R1$ = 0.0716, $wR2$ = 0.1450	
Largest diff. peak and hole	0.595 and -0.801 e.Å^{-3}	

Table S5. Crystal data and structure refinement for **[K(Crypt)][Fe(F)L$^{\mathbf{OCH2O}}$]**.

Identification code	brblh07	
Empirical formula	C48 H63 F Fe K N6 O15	
Formula weight	1077.99	
Temperature	100.00(10) K	
Wavelength	0.71073 Å	
Crystal system	orthorhombic	
Space group	$Pca2_1$	
Unit cell dimensions	a = 15.9303(3) Å	α = 90°
	b = 12.0821(3) Å	β = 90°
	c = 26.5119(8) Å	γ = 90°
Volume	5102.8(2) Å^3	
Z	4	
Density (calculated)	1.403 Mg/m^3	
Absorption coefficient	0.454 mm^{-1}	
F(000)	2268	
Crystal color, morphology	yellow, plate	
Crystal size	0.263 x 0.149 x 0.055 mm^3	
Theta range for data collection	1.536 to 33.052°	
Index ranges	$-23 \leq h \leq 22$, $-16 \leq k \leq 17$, $-39 \leq l \leq 39$	
Reflections collected	91122	
Independent reflections	16344 [R(int) = 0.0516]	
Observed reflections	12042	
Completeness to theta = 29.575°	100.0%	
Absorption correction	Multi-scan	
Max. and min. transmission	1.00000 and 0.62783	
Refinement method	Full-matrix least-squares on F^2	
Data / restraints / parameters	16344 / 634 / 893	
Goodness-of-fit on F^2	1.036	
Final R indices [I>2sigma(I)]	$R1$ = 0.0537, $wR2$ = 0.1264	
R indices (all data)	$R1$ = 0.0811, $wR2$ = 0.1364	
Absolute structure parameter	-0.006(5)	
Largest diff. peak and hole	0.561 and -0.353 e.Å^{-3}	

Table S6. Crystal data and structure refinement for **TBA[Fe(F)L$^{\mathbf{OMe}}$]**.

Identification code	brblh06	
Empirical formula	C49 H75 F Fe N5 O9	
Formula weight	952.99	
Temperature	100.00(11) K	
Wavelength	1.54184 Å	
Crystal system	monoclinic	
Space group	$P2_1/c$	
Unit cell dimensions	a = 29.0306(4) Å	α = 90°
	b = 23.0834(3) Å	β = 98.9191(11)°
	c = 15.06554(17) Å	γ = 90°
Volume	9973.7(2) Å^3	
Z	8	
Density (calculated)	1.269 Mg/m^3	
Absorption coefficient	2.932 mm^{-1}	
F(000)	4088	
Crystal color, morphology	yellow, needle	
Crystal size	0.5 x 0.061 x 0.019 mm^3	
Theta range for data collection	2.457 to 70.170°	
Index ranges	$-35 \leq h \leq 35$, $-28 \leq k \leq 10$, $-18 \leq l \leq 16$	
Reflections collected	75017	
Independent reflections	18819 [R(int) = 0.0686]	
Observed reflections	12855	
Completeness to theta = 67.684°	99.6%	
Absorption correction	Multi-scan	
Max. and min. transmission	1.00000 and 0.42092	
Refinement method	Full-matrix least-squares on F^2	
Data / restraints / parameters	18819 / 659 / 1540	
Goodness-of-fit on F^2	1.014	
Final R indices [I>2sigma(I)]	$R1$ = 0.0514, $wR2$ = 0.1229	
R indices (all data)	$R1$ = 0.0872, $wR2$ = 0.1406	
Largest diff. peak and hole	0.406 and -0.552 e.Å^{-3}	

S8. References

1. Armarego, L. L. F.; Chai, C. L. L. Purification of Laboratory Chemicals, 5th ed.; Elsevier, 2003.
2. C. D. Hastings, L. S. X. Huffman, C. K. Tiwari, J. G. Betancourth, W. W. Brennessel, and B. R. Barnett *Inorg. Chem.* 2023, **62**, 11920–11931.
3. C. D. Hastings, L. S. X. Huffman, W. W. Brennssel, and B. R. Barnett, *J. Am. Chem. Soc.* 2025, **147**, 14031–10435.
4. Sun, H.; DiMagno, S. G. *J. Am. Chem. Soc*. 2005, **127**, 2050–2051.
5. S. Stoll and A. Schweiger, *Mag. Res.*, 2006, **178**, 42.
6. a) F. Neese, F. Wennmohs, U. Becker, and C. Riplinger, The ORCA quantum chemistry program package. *The Journal of Chemical Physics*, 2020, **152**, 224108. b) F. Neese, Software update: The ORCA program system—Version 5.0. Wiley Interdiscipl. Rev. Comp. Mol. Sci., 2022, **12**, e1606.
7. N. C. Handy and A. J. Cohen, Left-Right Correlation Energy. *Mol. Phys.* 2001, **99**, 403–412.
8. S. Grimme, J. Antony, S. Ehrlich, and H. Krieg *J. Chem. Phys.* 2010, **132**, 154104.
9. F. Weigend and R. Ahlrichs, *Phys. Chem. Chem. Phys.* 2005, **7**, 3297–3305.
10. F. Weigend *Phys. Chem. Chem. Phys.* 2006, **8**, 1057–1065.
11. S. Alvarez, *Dalton Trans.* 2013, **42**, 8617–8636.
12. CrysAlisPro, version 171.42.72a; Rigaku Corporation: Oxford, UK, 2022.
13. Sheldrick, G. M. SHELXT, version 2018/2; Acta. Crystallogr. 2015, A71, 3–8.
14. Sheldrick, G. M. SHELXL, version 2019/2; Acta. Crystallogr. 2015, C71, 3–8.
15. Dolomanov, O. V.; Bourhis, L. J.; Gildea, R. J.; Howard, J. A. K.; Puschmann, H. Olex2, version 1.5; *J. Appl. Cryst*. 2009, **42**, 339–341.